INFECTION AND IMMUNITY, Sept. 2009, p. 4150–4160 Vol. 77, No. 9
0019-9567/09/$08.00+0 doi:10.1128/IAI.00683-09

BAR Domain Proteins Rvs161 and Rvs167 Contribute to *Candida albicans* Endocytosis, Morphogenesis, and Virulence[▽]

Lois M. Douglas, Stephen W. Martin,† and James B. Konopka*

Department of Molecular Genetics and Microbiology, Stony Brook University, Stony Brook, New York 11794-5222

Received 15 June 2009/Returned for modification 29 June 2009/Accepted 7 July 2009

The *Candida albicans* plasma membrane plays critical roles in growth and virulence and as a target for antifungal drugs. Three *C. albicans* genes that encode Bin-Amphiphysin-Rvs homology domain proteins were mutated to define their roles in plasma membrane function. The deletion of *RVS161* and *RVS167*, but not *RVS162*, caused strong defects. The *rvs161*Δ mutant was more defective in endocytosis and morphogenesis than *rvs167*Δ, but both were strongly defective in polarizing actin patches. Other plasma membrane constituents were still properly localized, including a filipin-stained domain at the hyphal tips. An analysis of growth under different in vitro conditions showed that the *rvs161*Δ and *rvs167*Δ mutants grew less invasively in agar and also suggested that they have defects in cell wall synthesis and Rim101 pathway signaling. These mutants were also more resistant to the antimicrobial peptide histatin 5 but showed essentially normal responses to the drugs caspofungin and amphotericin. Surprisingly, the *rvs161*Δ mutant was more sensitive to fluconazole, whereas the *rvs167*Δ mutant was more resistant, indicating that these mutations cause overlapping but distinct effects on cells. The *rvs161*Δ and *rvs167*Δ mutants both showed greatly reduced virulence in mice. However, the mutants were capable of growing to high levels in kidneys. Histological analyses of infected kidneys revealed that these *rvs*Δ mutants grew in a large fungal mass that was walled off by leukocytes, rather than forming disseminated microabscesses as seen for the wild type. The diminished virulence is likely due to a combination of the morphogenesis defects that reduce invasive growth and altered cell wall construction that exposes proinflammatory components to the host immune system.

Candida albicans is the most common human fungal pathogen and causes a wide range of infections in susceptible individuals (31). One characteristic of *C. albicans* is that the host milieu stimulates it to grow in different morphologies, including rounded buds, elongated pseudohyphae, and long filamentous hyphae (39). The induction of the hyphal form also correlates with the increased expression of virulence factors, such as adhesins that promote attachment to human cells and biofilm formation, secreted hydrolytic enzymes that may liberate nutrients and facilitate invasive growth, and antioxidant enzymes that counter the attack of the immune system (5, 7, 21, 47). The *C. albicans* plasma membrane plays special roles during these important morphological transitions. In addition to forming an important protective barrier, the plasma membrane contains components that sense the extracellular environment, induce changes in morphogenesis, and mediate virulence factor production. The plasma membrane is also involved in dynamic cellular processes, such as endocytosis and cell wall biogenesis. Consistent with its key role in infection, the plasma membrane is a target of most of the commonly used antifungal drugs (32).

Studies of *Saccharomyces cerevisiae* have shown that endocytosis contributes to environmental sensing and morphogenesis. The plasma membrane is not static, but rather it is continuously remodeled by the endocytic internalization of membrane constituents (13). Endocytosed lipids and proteins can be recycled back to the plasma membrane or sent to the vacuole for degradation. The stability of many nutrient receptors and transporters in the plasma membrane is regulated by endocytosis in response to changes in nutrient levels (18). Other signal transduction components can also be regulated by endocytosis, such as the ligand-induced internalization of mating pheromone receptors. Endocytosis is also thought to contribute to polarized morphogenesis by internalizing components and reinserting them at the site of cell polarization (40).

A large number of proteins contribute to the complex process of endocytosis. The roles of these proteins have been most well studied for *S. cerevisiae*, for which four different protein modules involved in the internalization process have been defined (19). Endocytic site assembly begins with the localization of clathrin and the formation of a coat complex in a module that also includes Pan1, End3, Sla1, and Sla2. The WASP/MYO module (Las17 and later Myo5) then interacts with the actin module ARP2/ARP3 complex to initiate actin polymerization, which drives the internalization of the actin-bound coat and attached membrane and cargo. The fourth module is comprised of the Rvs161 and Rvs167 amphiphysin homologs that bind to the invaginating tubule and promote scission to separate the vesicle from the basal plasma membrane. The trafficking of the released vesicle to its final destination then continues along actin cables within the cytoplasm.

In order to study the roles of plasma membrane organization and endocytosis in *C. albicans*, we analyzed the orthologs of the *S. cerevisiae RVS161* and *RVS167* (*ScRVS161* and *ScRVS167*, respectively) genes. The deletion of *RVS161* and *RVS167* in *S. cerevisiae* causes a defect in the internalization

* Corresponding author. Mailing address: Department of Molecular Genetics and Microbiology, Stony Brook University, Stony Brook, NY 11794-5222. Phone: (631) 632-8715. Fax: (631) 632-9797. E-mail: jkonopka@ms.cc.sunysb.edu.

† Present address: Cell Surface Signaling Lab, Wellcome Trust Genome Campus, Hinxton, Cambridge, CB10 1SA, United Kingdom.

▽ Published ahead of print on 13 July 2009.

TABLE 1. *C. albicans* strains used in this study

Strain	Parent	Genotype
BWP17	Sc5314	*ura3*Δ::λ*imm434 ura3*Δ::λ*imm434 his1*::*hisG his1*::*hisG arg4*::*hisG arg4*::*hisG*
DIC185	BWP17	*ura3*Δ::λ*imm434 URA3 his1*::*hisG HIS1 arg4*::*hisG ARG4*
YSM42	BWP17	BWP17, except *rvs161*Δ::*ARG4 rvs161*Δ::*HIS1*
YLD14	YSM42	BWP17, except *rvs161*Δ::*ARG4 rvs161*Δ::*HIS1 ura3*Δ::λ*imm434 URA3*
YLD11	YSM42	BWP17, except *rvs161*Δ::*ARG4 rvs161*Δ::*HIS1 RVS161*::*URA3*
YSM37	BWP17	BWP17, except *RVS161-HA*::*URA3*
YLD26	YSM42	BWP17, except *rvs161*Δ::*ARG4 rvs161*Δ::*HIS1 CDC12-GFP*::*URA3*
YLD29	YSM42	BWP17, except *rvs161*Δ::*ARG4 rvs161*Δ::*HIS1* SUR7-GFP::URA3
YLD21	BWP17	BWP17, except *rvs162*Δ::*ARG4 rvs162*Δ::*HIS1*
YLD22	YLD21	BWP17, except *rvs162*Δ::*ARG4 rvs162*Δ::*HIS1 ura3*Δ::λ*imm434*/*URA3*
YLD25	YLD21	BWP17, except *rvs162*Δ::*ARG4 rvs162*Δ::*HIS1 RVS162*::*URA3*
YLD19	BWP17	BWP17, except *RVS162-HA*::*URA3*
YLD28	YLD21	BWP17, except *rvs162*Δ::*ARG4 rvs162*Δ::*HIS1 CDC12-GFP*::*URA3*
YLD31	YLD21	BWP17, except *rvs162*Δ::*ARG4 rvs162*Δ::*HIS1 SUR7-GFP*::*URA3*
YLD3	BWP17	BWP17, except *rvs167*Δ::*ARG4 rvs161*Δ::*HIS1*
YLD16	YLD3	BWP17, except *rvs167*Δ::*ARG4 rvs161*Δ::*HIS1 ura3*Δ::λ*imm434 URA3*
YLD12	YLD3	BWP17, except *rvs167*Δ::*ARG4 rvs161*Δ::*HIS1 RVS167*::*URA3*
YSM54	BWP17	BWP17, except *RVS167-HA*::*URA3*
YLD27	YLD3	BWP17, except *rvs167*Δ::*ARG4 rvs161*Δ::*HIS1 CDC12-GFP*::*URA3*
YLD30	YLD3	BWP17, except *rvs167*Δ::*ARG4 rvs161*Δ::*HIS1 SUR7-GFP*::*URA3*
YJA15	BWP17	BWP17, except *SUR7-GFP*::*URA3*

phase of endocytosis with less impairment of actin function and morphogenesis than was seen with many other endocytic mutants (24, 28). The *S. cerevisiae RVS* genes were initially identified because their mutation caused a *r*educed *v*iability upon *s*tarvation (10). Subsequent studies revealed that the Rvs proteins contain a BAR (*B*in-*A*mphiphysin-*R*vs) homology domain, which has been shown in other organisms to sense and promote membrane curvature (12, 52). The *S. cerevisiae rvs* mutants also display other phenotypes that may be directly or indirectly linked to their endocytosis defect, including a defect in vesicle trafficking, increased sensitivity to high salt, and decreased cell wall integrity (4, 6). The Rvs161 and Rvs167 proteins have been isolated in a detergent-resistant membrane fraction, which suggests that they localize in ergosterol- and sphingolipid-enriched plasma membrane domains that are similar to lipid rafts (16). We therefore mutated *RVS161* and *RVS167* in *C. albicans* (*CaRVS161* and *CaRVS167*, respectively), along with a third uncharacterized BAR domain gene exhibiting similarity to *S. cerevisiae RVS161*, which we have termed *RVS162*. The results demonstrate that *CaRVS161* and *CaRVS167*, but not *CaRVS162*, are important for efficient endocytosis, true hyphal filamentation, and virulence in a mouse model of hematogenously disseminated candidiasis.

MATERIALS AND METHODS

Strains and media. The *C. albicans* strains used in this study (Table 1) were grown in rich yeast extract-peptone-dextrose (YPD) medium with uridine (80 mg/liter) or in synthetic medium lacking the indicated nutrients (38). Homozygous mutant strains were constructed from the parental BWP17 strain by the sequential deletion of both copies of the targeted gene (*C. albicans* is diploid). Gene deletion cassettes were generated by PCR amplification of the *ARG4* or *HIS1* selectable marker genes using primers that also included 60 bp of DNA sequence homologous to the upstream or downstream regions of the targeted open reading frame (49). Cells which had undergone homologous recombination to delete the targeted gene were identified by PCR analysis using a combination of primers flanking sites of cassette integration and internal primers. Reconstituted strains in which the deletion mutations were complemented by the reintroduction of a wild-type copy of the targeted gene were constructed by integrating a plasmid containing the gene of interest and the *URA3* selectable marker into the 5′ region of the deleted gene. Briefly, the entire open reading frame plus ~1,000 bp upstream and 300 bp downstream were amplified by PCR and inserted into the SacI and SacII restriction sites in the plasmid pDDB57 (48). Prior to transformation into *C. albicans* deletion strains, complementing plasmids were linearized by restriction digestion in the promoter region for targeted integration.

The *rvs* deletion strains used in virulence assays were transformed with a *URA3*-containing fragment to complement the remaining auxotrophy. The plasmid pBSK-*URA3* (33) was digested with restriction enzymes PstI and NotI to liberate the *URA3-IRO1* sequence, which was then transformed into the mutant strains for integration by homologous recombination to restore *URA3* at its native locus.

The *RVS* genes were tagged by the insertion of the hemagglutinin (HA) epitope via homologous recombination at the C-terminal coding region of each gene with a HA-*URA3* cassette. The HA-*URA3* cassette was created by PCR amplification using primers directed to the p3xHA plasmid (26) that were flanked by 60 to 80 bp of sequence homologous to the regions surrounding the stop codon. *RVS* deletion strains containing the *SUR7-GFP* fusion gene (where *GFP* is the green fluorescent protein gene) were derived by transformation with a DNA fragment containing *SUR7-GFP* and the *URA3* selectable marker that was created by PCR amplification of the corresponding DNA using strain YJA15 as a template and 23-bp primers designed to anneal ~500 bp upstream and downstream of the *SUR7* open reading frame stop codon. Plasmid pAW-*CDC12*-GFP (45) was linearized with restriction enzyme BsaB1 and transformed into the strains for the targeted integration of GFP at the C terminus of *CDC12*.

Western blotting. Log-phase cells were lysed by agitation with glass beads for 1 min in the presence of lysis buffer (20 mM Tris [pH 7.5], 100 mM NaCl, 1 mM EDTA) and protease inhibitors (1 μg/ml pepstatin, 1 mM benzamidine, 0.5 mM phenylmethylsulfonyl fluoride). Protein levels in the extracts were quantified by a modified Bradford assay (Pierce Biotechnology, Inc.), and 100 μg of protein was separated by sodium dodecyl sulfate-polyacrylamide gel electrophoresis and then transferred to a nitrocellulose membrane (Whatman International Limited). The filters were incubated in blocking solution (5% powdered milk, 10 mM Tris [pH 7.5], 150 mM NaCl) and then incubated overnight at 4°C with anti-HA rabbit polyclonal antibody (Bethyl Laboratories, Montgomery, TX), followed by incubation in anti-rabbit horseradish peroxidase-conjugated antibody. The chemiluminescent detection of the cross-reacting bands was performed using a SuperSignal West Dura kit (Pierce Biotechnology, Inc.).

Fluorescence microscopy. For the assessment of endocytosis, log-phase cells were incubated for 15 min on ice with the lipophilic fluorescent dye FM4-64 (Invitrogen, Carlsbad, CA) at a concentration of 20 μM (42). The cells were then washed, resuspended in fresh medium, and evaluated by fluorescence microscopy at 15, 30, and 60 min for dye internalization and staining of the vacuolar membrane. For actin localization (1), log-phase cells were initially fixed in 5% formaldehyde for 75 min at 30°C, followed by incubation at room temperature for 30

min in 0.1 M potassium phosphate buffer (pH 7.5) containing 0.1% Triton X-100. After the cells were washed two times in 0.1 M potassium phosphate buffer (pH 7.5), five units of rhodamine-phalloidin (Invitrogen, Carlsbad, CA) were added and the cells incubated at 4°C overnight in the dark. The cells were washed three times in 0.1 M potassium phosphate buffer (pH 7.5) and then resuspended in mounting medium containing 10 μg/ml phenylenediamine (Sigma) and examined microscopically. Fluorescent staining of cell wall chitin was carried out by incubating the cells in 100 to 500 μl of 20 ng/ml calcofluor white (Fluorescent Brightener 28; Sigma) for ~10 min at room temperature and then viewing by fluorescence microscopy (34). Ergosterol was stained by incubating cells with 10 to 20 μg/ml filipin complex (Sigma) for 5 min, and then the cells were examined immediately by fluorescence microscopy using a DAPI (4′-6-diamidino-2-phenylindole) filter set (2, 25).

Virulence assays. *C. albicans* strains were grown overnight at 30°C in YPD medium with 80 mg/liter uridine, reinoculated into fresh medium the next day, and incubated again overnight at 30°C. Mutant strain cultures were sonicated for 5 s to break up aggregates, and then the cells were washed twice in phosphate-buffered saline (PBS), counted in a hemocytometer, and diluted to 1×10^7 cells/ml with PBS. Dilutions of cells were plated onto solid YPD medium plates to confirm the quantitation. Eight female BALB/c mice were inoculated per each *C. albicans* strain with 1×10^6 cells into the lateral tail vein of each mouse. The mice were monitored for 28 days, during which time a mouse was considered moribund if food and water could no longer be accessed. Humane euthanasia was then performed. For an analysis of the early stages of infection, infected mice were euthanized after 2 or 3 days, as indicated in Fig. 8. Graphing and statistical analysis of survival after infection was carried out using a log-rank test (Mantel-Haenszel test) with Prism 4 (GraphPad Software, Inc., La Jolla, CA). Kidneys excised for fungal burden assessment were weighed, placed in 5 ml PBS, and homogenized for 30 s with a tissue homogenizer (Pro Scientific, Inc., Oxford, CT). Serial dilutions of the homogenate were plated onto YPD medium plates and incubated at 30°C for 2 days to determine the number of CFU per gram of kidney tissue. Statistical analysis of the CFU data was carried out with Prism software using one-way analysis of variance with a nonparametric Kruskal-Wallis test and a Dunn's posttest. Periodic acid-Schiff (PAS) and hematoxylin-eosin staining for histological analysis were performed by a commercial laboratory (McLain Laboratories, Smithtown, NY). Calcofluor white staining was carried out on kidney tissue by pelleting 500 μl of homogenate and then resuspending it in 100 to 500 μl of 20 ng/ml calcofluor white for ~10 min. The stained tissue was then resuspended in 1% KOH, incubated for 5 min at room temperature, and examined by fluorescence microscopy.

Antifungal susceptibility. Etest gradient strips (AB Biodisk, Solna, Sweden) were used to assess the sensitivity of the *C. albicans* strains to amphotericin B, fluconazole, and caspofungin essentially as recommended by the manufacturer. Strains were grown overnight in YPD medium plus 80 mg/liter uridine at 30°C and then diluted to 1×10^6 cells/ml. A total of 250 μl of cells was then spread onto solid RPMI 1640 medium containing glutamine and buffered to pH 7.0 with 165 mM morpholinepropanesulfonic acid. The surface of each plate was allowed to dry, and then Etest strips were applied. The plates were incubated at 30°C, and the MIC was recorded at 24 and 48 h as the lowest level at which the elliptical zone of growth inhibition intersected with the strip. Susceptibility to histatin 5 (Hst 5) was tested with strains grown overnight in YPD medium at 30°C, washed two times in 10 mM sodium phosphate buffer (pH 7.4), and then diluted to 2.5×10^5 cells/ml (22). A total of 20 μl (5,000 cells) were then added to 20 μl of the indicated concentration of Hst 5 (Sigma-Aldrich) in low-retention tubes. The reactions were incubated for 90 min at 37°C with shaking at 250 rpm, followed by dilution with 360 μl of 10 mM sodium phosphate buffer. A total of 30 μl was then spread onto a YPD medium plate and incubated at 30°C for 48 h. The number of CFU was then assessed and the percentage of loss of viability calculated as 1 − (Hst 5 CFU/control CFU) (22).

RESULTS

Three Rvs proteins produced in *C. albicans*. Protein similarity searches revealed that *C. albicans* encodes three BAR domain family proteins (Fig. 1). Two are similar to *S. cerevisiae* Rvs161 and Rvs167, and the third protein lacks an ortholog in *S. cerevisiae* (orf19.6349). We named this new protein Rvs162, since it is more closely related to Rvs161 (~35% identity). Rvs162 is also similar to Rvs161 in that it lacks the GPA and SH3 domains present in Rvs167, which are thought to mediate interaction with other proteins (14, 15). RVS162 orthologs were detected in other fungal genomes that are more closely related to *C. albicans* (e.g., *Debaryomyces hansenii*).

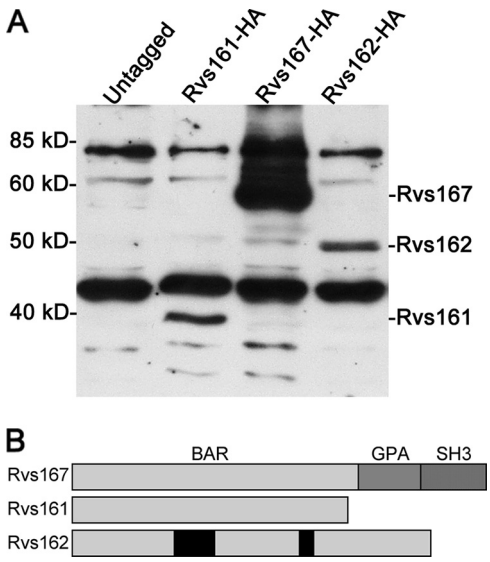

FIG. 1. The Rvs161, Rvs167, and Rvs162 proteins are produced by *C. albicans*. (A) Western blot analysis of an untagged control *C. albicans* strain (DIC185) and the following strains in which the indicated *RVS* gene was tagged with a triple HA epitope at the 3′ end of the open reading frame: YSM37 (*RVS161*-HA), YLD19 (*RVS162*-HA), and YSM54 (*RVS167*-HA). (B) Diagram of Rvs protein structures. Rvs161, Rvs167, and Rvs162 each contain an N-terminal BAR domain. Rvs167 also has an internal glycine-, proline-, and alanine-rich sequence (GPA), followed by a C-terminal SH3 domain.

To confirm the production of the Rvs proteins in *C. albicans*, one allele of each gene was tagged with a triple HA epitope. One of the two *RVS162* alleles contains numerous mutations (orf19.13706 genome sequence and our unpublished data), including a frameshift that causes a premature truncation of the open reading frame, so we tagged the other allele (orf19.6349), which contains an open reading frame across the whole BAR domain. Western blots revealed that all three Rvs proteins were produced by budding cells (Fig. 1A) and by cells induced with serum to form hyphae (data not shown). The gel mobilities of the proteins were similar to the sizes of the predicted proteins (Rvs161, 34 kDa; Rvs162, 39.4 kDa; Rvs167, 53.3 kDa) plus the additional mass of the 3× HA tag. Rvs167 was consistently produced at higher levels than Rvs161 or Rvs162. Rvs167 also exhibited additional forms with lower gel mobility, possibly due to the phosphorylation of sites within the putative GPA domain as has been reported for *S. cerevisiae* Rvs167 (Fig. 1B) (15).

Altered morphogenesis and growth properties of *rvs161*Δ and *rvs167*Δ mutants. Homozygous deletion mutants of the three *RVS* genes were constructed for *C. albicans* strain BWP17 (see Materials and Methods). The *rvs161*Δ and *rvs167*Δ cells displayed slight defects in bud morphogenesis, forming somewhat larger, rounder buds than the wild type and an increase in the random budding pattern (Fig. 2A). The defects were complemented by the reintroduction of the corresponding wild-type *RVS* gene. The *rvs161*Δ and *rvs167*Δ mutants displayed increased sensitivity to calcofluor white and

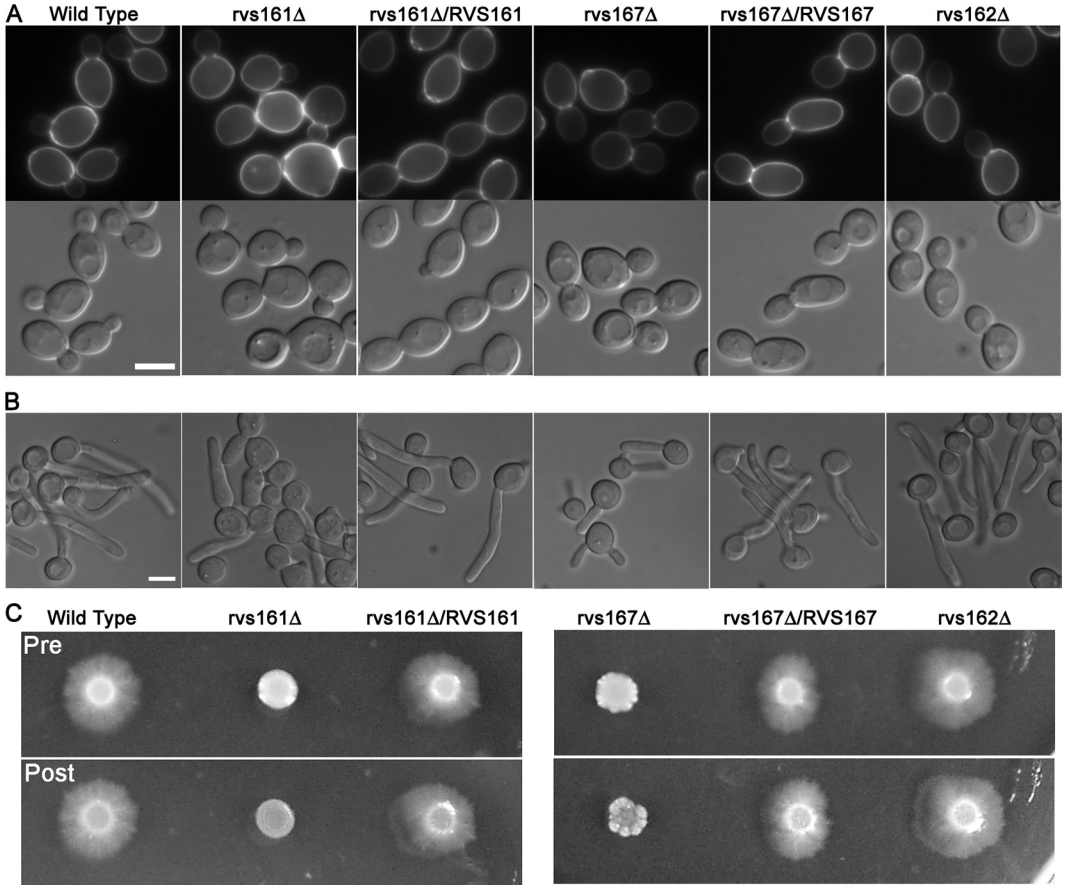

FIG. 2. *Carvs161*Δ and *Carvs167*Δ exhibit defects in morphology. (A) Morphology of log-phase yeast-form cells grown in YPD medium plus uridine at 30°C. Calcofluor white-stained cells are shown in the top panels and DIC images in the bottom panels. The *rvs161*Δ and *rvs167*Δ cultures contained a greater level of large, round mother cells than the wild-type or complemented strains, to which a single copy of the corresponding *RVS* open reading frame was restored. (B) Morphology of cells grown under hyphal-inducing conditions in liquid medium (YPD plus 10% bovine calf serum for 75 min at 37°C). *rvs161*Δ and *rvs167*Δ, but not *rvs162*Δ, exhibited defects in hyphal growth. *rvs161*Δ formed predominantly pseudohyphae, while *rvs167*Δ produced both pseudohyphae and true hyphal filaments. However, the development of *rvs167*Δ filaments was slower than that of the wild-type and complemented strain filaments. (C) Defects of the *rvs161*Δ and *rvs167*Δ mutants when grown on solid-medium agar plates containing 4% bovine calf serum to stimulate invasive hyphal growth. Plates were incubated for 7 days at 37°C. The top and bottom panels show the plate before and after washing to remove the noninvasive cells. Strains used were YLD14 (*rvs161*Δ), YLD22 (*rvs162*Δ), YLD16 (*rvs167*Δ), YLD11 (*rvs161*Δ/*rvs161*Δ/*RVS161*), YLD12 (*rvs167*Δ/*rvs167*Δ/*RVS167*), and wild-type DIC185.

Congo red, which indicates they have altered cell walls and suggests they may have a defect in chitin synthesis (Table 2). However, the mutants were not generally defective in cell wall synthesis, since they were not more sensitive to growth in the presence of high salt (1.5 M NaCl), 0.5 M $CaCl_2$, or 0.06% sodium dodecyl sulfate. The *Carvs161*Δ and *Carvs167*Δ mutants were also very sensitive to 150 mM LiCl and weakly sensitive to growth under an alkaline pH, suggesting that they may have defects in the activation of the RIM101 pathway similar to those of other endocytosis mutants (11, 20). Both the *Carvs161*Δ and *Carvs167*Δ mutants were more sensitive to 5 mM H_2O_2, with *Carvs167*Δ being the most sensitive. In contrast, the deletion of *CaRVS162* did not cause detectable effects. Surprisingly, the *Carvs*Δ mutants differed from the *Scrvs*Δ mutants (10) in that they did not display reduced viability upon starvation, even after incubation for 8 weeks in water.

Hyphal morphogenesis was examined by inducing cells with 10% bovine calf serum at 37°C (Fig. 2B). Interestingly, the

TABLE 2. Growth phenotypes of *C. albicans rvs*Δ mutants under different conditions[a]

Condition	Wild type	*rvs161*Δ	*rvs162*Δ	*rvs167*Δ
NaCl (1.5 M)	+++	+++	+++	+++
$CaCl_2$ (0.5 M)	+++	+++	+++	+++
LiCl (0.15 M)	+++	−	+++	−
Calcofluor white (40 μg/ml)	+++	+	+++	++
Congo red (100 μg/ml)	+++	+	+++	+
Sodium dodecyl sulfate (0.06%)	+++	++	+++	+++
HEPES (pH 8.5; 150 mM)	+++	++	+++	++/+++
H_2O_2 (5 mM)	+++	++	+++	+
8-wk starvation[b]	+++	+++	+++	+++

[a] Dilutions of cells were spotted on the indicated plates, and then relative growth was recorded. Growth relative to the wild-type strain under each condition is indicated as follows: +++, >30% of that of the wild type; ++, 3% to 30% of that of the wild type; +, 0.3% to 3% of that of the wild type; and −, no growth.

[b] wk, week. *rvs161*Δ grew more slowly coming out of the stationary phase but did not display reduced viability.

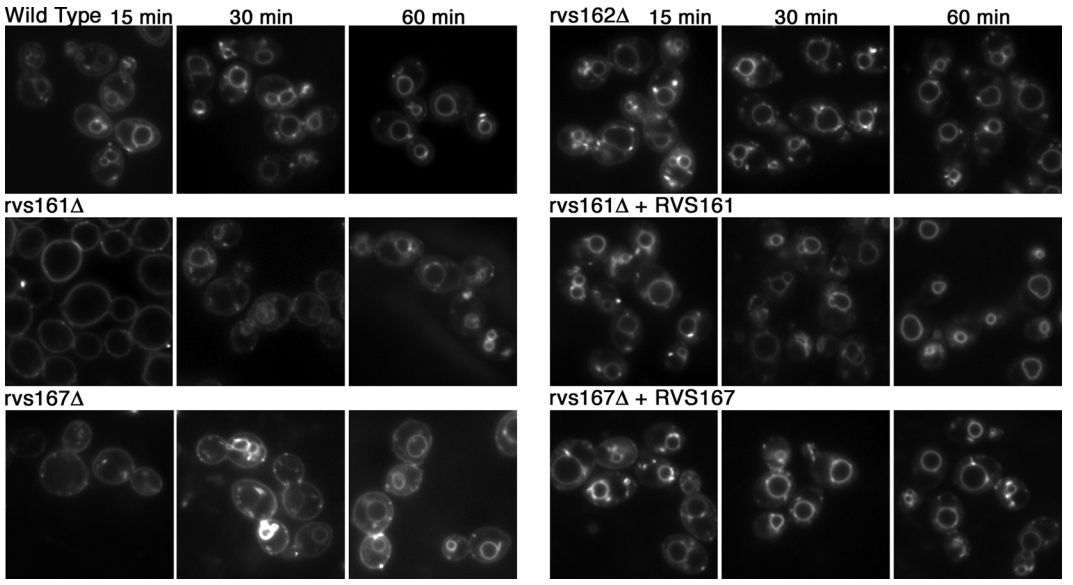

FIG. 3. *Carvs161*Δ and *Carvs167*Δ, but not *Carvs162*Δ, exhibit defects in endocytosis. Log-phase cells were incubated in 20 μM FM4-64 on ice for 15 min and monitored for internalization of the stain after incubation at 30°C for 15, 30, and 60 min. *rvs161*Δ exhibited the greatest defect, with little or no internalization of the stain after 15 min, while *rvs167*Δ demonstrated both surface staining and some staining of endocytic intermediates and the vacuolar membrane. However, after 60 min, both *rvs161*Δ and *rvs167*Δ cells displayed an increased ring pattern indicative of vacuolar membrane staining. The deletion of *RVS162* resulted in endocytic internalization similar to that of the wild-type strain. The strains used were wild-type DIC185, YLD14 (*rvs161*Δ), YLD22 (*rvs162*Δ), YLD16 (*rvs167*Δ), YLD11 (*rvs161*Δ/*rvs161*Δ/*RVS161*), and YLD12 (*rvs167*Δ/*rvs167*Δ/*RVS167*).

*rvs161*Δ mutant was strongly defective and developed chiefly pseudohyphal-type forms. The *rvs167*Δ mutant formed hyphae that appeared more similar to those of the wild type, but the hyphal growth was slower to develop. The *rvs162*Δ mutant formed hyphae similar to those of the wild type (Fig. 2B). Thus, the different *RVS* genes make distinct contributions to hyphal morphogenesis. Consistent with their altered morphogenesis, the *rvs161*Δ and *rvs167*Δ mutants grew less invasively in agar (Fig. 2C).

Endocytosis defects of the *C. albicans rvs161*Δ and *rvs167*Δ mutants. The endocytic capacity of the *Carvs* mutants was examined by assaying their ability to internalize the lipophilic dye FM4-64. As expected for the wild-type control strain (DIC185), the plasma membrane was no longer stained after 15 min of incubation, and instead, a ring pattern of intracellular staining appeared, indicating that FM4-64 was efficiently endocytosed and localized in the vacuolar membrane (Fig. 3). Similar results were observed for the *rvs162*Δ mutant. In contrast, FM4-64 staining was still confined to the plasma membrane of the *rvs161*Δ strain after 15 min. The *rvs167*Δ mutant gave an intermediate phenotype, with faint staining of the vacuole and endocytic intermediates in addition to plasma membrane staining. By 60 min, both mutants demonstrated increased vacuolar staining, indicating that trafficking to the vacuole still occurred, albeit at a slower rate (Fig. 3). Similar defects were observed in mutant strains induced for hyphal growth (data not shown). The endocytosis defects were complemented by the reintroduction of a wild-type copy of the corresponding gene.

Actin polarization defects in the *rvs161*Δ and *rvs167*Δ mutants. Rhodamine-phalloidin staining of budding cells to detect filamentous actin revealed the expected cortical actin patches localized to the growing buds in the control strain DIC185 and in *rvs162*Δ (Fig. 4A). In contrast, the *rvs161*Δ and *rvs167*Δ mutants showed extensive mislocalization of actin patches to the mother cells, similar to the corresponding *S. cerevisiae* mutants (28). Also, fewer actin cables were detected in the mutants. This correlates with a larger, rounder bud morphology that was most obvious in the *Carvs161*Δ cells (Fig. 2A). The actin localization defects were complemented by the reintroduction of a wild-type copy of the corresponding gene.

Wild-type cells induced with 10% serum showed strong polarization of actin patches to the hyphal tip. In contrast, actin patches were mislocalized throughout the *rvs161*Δ and *rvs167*Δ mutant hyphae (Fig. 4B). Interestingly, actin cables could still be detected projecting from the leading edge of growth in the mutant cells. Although there were fewer cables detected than in the wild-type hyphae, the actin cables presumably help promote the degree of hyphal growth that is detected in these mutants.

***rvs161*Δ cells exhibit polarized filipin staining of ergosterol at the leading edge of hyphal growth.** The ability of the *rvs*Δ mutants to undergo polarized hyphal growth was defined further by staining cells with filipin, an autofluorescent polyene antibiotic that binds ergosterol (2). Filipin stains the leading edge of hyphal growth, but not buds or pseudohyphae, suggesting that this distinct lipid composition contributes to highly polarized growth at the hyphal tips (25). Although *rvs161*Δ cells displayed the strongest endocytosis defect, they still exhibited increased filipin staining at polarized sites of growth after a short 30-min induction in 10% serum (Fig. 5). Similar results were observed for the *rvs167*Δ and *rvs162*Δ mutants (data not shown). After 75 min of incubation in serum, increased filipin staining was seen at the leading edge of growth

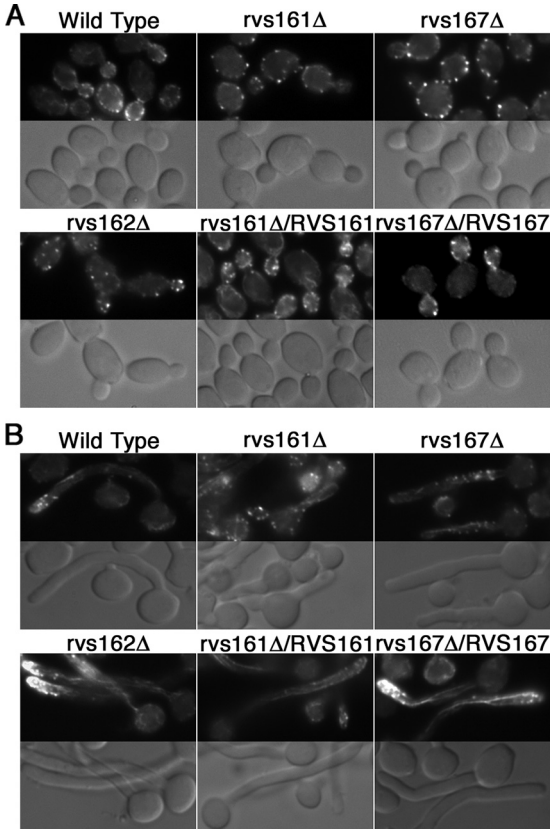

FIG. 4. Actin polarization defects of *rvs161*Δ and *rvs167*Δ strains. Actin localization in budding cells (A) and cells induced to form hyphae (B) by growth in medium containing 10% bovine calf serum at 37°C. Wild-type strain DIC185 and the indicated *rvs*Δ mutant strains were analyzed by staining fixed cells with rhodamine-conjugated phalloidin (top panels) and by DIC light microscopy (bottom panels). The deletion of *RVS161* and *RVS167* resulted in the increased appearance of actin patches on the mother cell surface with few cables. The *rvs162*Δ strain appeared similar to the wild-type and complemented strains in which the corresponding wild-type *RVS* gene was reintroduced. Strains used were YLD14 (*rvs161*Δ), YLD22 (*rvs162*Δ), YLD16 (*rvs167*Δ), YLD11 (*rvs161*Δ/*rvs161*Δ/*RVS161*), and YLD12 (*rvs167*Δ/*rvs167*Δ/*RVS167*).

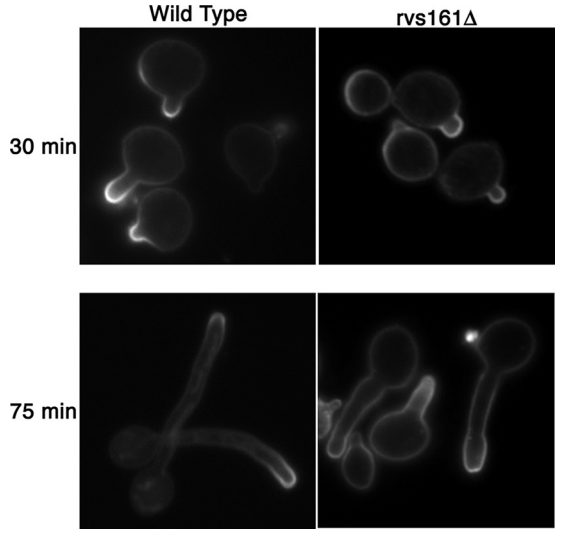

FIG. 5. Polarized filipin staining of ergosterol in *rvs161*Δ grown under hyphal-inducing conditions. Wild-type DIC185 and YLD14 (*rvs161*Δ) cells were stimulated with 10% bovine calf serum at 37°C for 30 and 75 min, stained with filipin, and then immediately examined by fluorescence microscopy. *rvs161*Δ cells exhibited increased filipin staining of ergosterol at the leading edges of growth similar to the wild type at both 30 and 75 min.

in the *rvs161*Δ mutant similar to that of the wild type, even in cells with a pseudohyphal morphology. Thus, the formation of acute hyphal projections is not required for polarized filipin staining. Altogether, these assays indicate that efficient endocytosis is not essential for the altered plasma membrane structure of hyphal tips. Additional studies showed that the *rvs*Δ mutations did not affect the localization of plasma membrane proteins that are thought to be present in other specialized lipid domains (data not shown), including the localization of Sur7-GFP to punctate patches in the plasma membrane (3) or the localization of septin proteins to the bud neck (8).

Altered sensitivity to fluconazole and Hst 5. The *rvs*Δ mutants were tested for sensitivity to antifungal drugs that target plasma membrane functions (32) using Etest strips, which release a gradient of drug that diffuses into a solid medium agar plate (Fig. 6). The mutant strains showed essentially the wild-type response to caspofungin and amphotericin B (data not shown). In contrast, *rvs161*Δ was more sensitive to fluconazole, which blocks an intermediate step in ergosterol synthesis (32). The MIC was approximately fivefold lower for *rvs161*Δ. Similar results were observed for cells grown in liquid cultures (data not shown). Surprisingly, the *rvs167*Δ mutant was more resistant to fluconazole (Fig. 6). However, there was always lighter growth surrounding the Etest strip, indicating partial sensitivity to lower doses of fluconazole. Liquid broth micro- and macrodilution assays (37) confirmed that the partial inhibition of *rvs167*Δ occurred at lower doses than for the wild type but that the *rvs167*Δ mutant was also capable of growing, albeit more slowly, at doses of fluconazole that were ≥50-fold higher than the dose that inhibited the wild type. The different sensitivities of the *rvs161*Δ and *rvs167*Δ mutants to fluconazole indicate that these phenotypes do not correlate with the overall endocytosis defects and suggest that this may be due to another function of the Rvs proteins.

The *rvs*Δ mutants were also tested for sensitivity to the antimicrobial peptide Hst 5, which is secreted by acinar cells of the human parotid glands into the oral cavity (36). Interestingly, both *rvs161*Δ and *rvs167*Δ exhibited increased resistance to Hst 5 compared with that of the wild-type and *rvs162*Δ strains (Fig. 6B). The half-maximal response (50% effective concentration) indicated that *rvs161*Δ was 5.9-fold more resistant to Hst 5 and *rvs167*Δ was 10.3-fold more resistant. Efficient endocytosis may play a direct role in the fungicidal activity of Hst 5 by promoting its internalization into cells. However, the role of the Rvs proteins could also be indirect, due to changes in lipid composition or the physical properties of the plasma membrane (27, 41).

***rvs161*Δ and *rvs167*Δ exhibit attenuated virulence.** The pathogenicity of the *rvs* mutants was examined in a mouse model of hematogenously disseminated candidiasis. As expected, BALB/c mice injected with the wild-type control strain

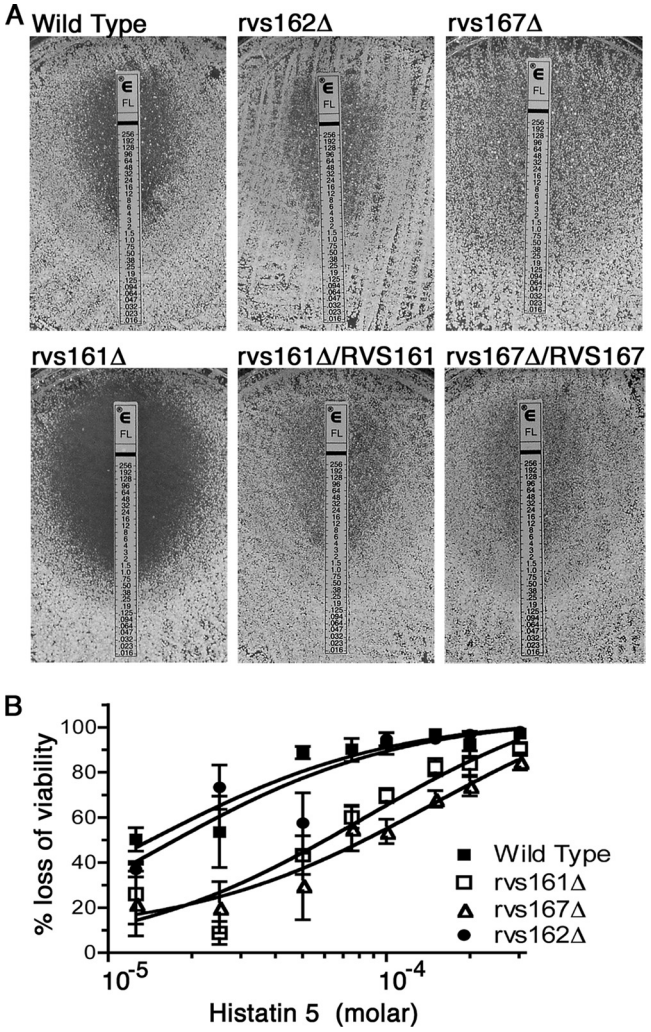

FIG. 6. Altered responses of *rvs*Δ mutants to antifungal agents. (A) Increased susceptibility of *rvs161*Δ mutant to fluconazole. The indicated cells were spread onto solid RPMI medium, and then an Etest strip was applied to the agar surface to generate a gradient of fluconazole. *rvs161*Δ demonstrated increased susceptibility to fluconazole at 48 h, with no growth within the ellipse of inhibition, unlike the wild-type, *rvs167*Δ, or *rvs162*Δ strain or a strain in which *rvs161*Δ was complemented by the introduction of one copy of *RVS161*. Strains used were YLD14 (*rvs161*Δ), YLD22 (*rvs162*Δ), YLD16 (*rvs167*Δ), YLD11 (*rvs161*Δ/*rvs161*Δ/*RVS161*), and wild-type DIC185. (B) Cells were incubated at 37°C with the indicated concentration of Hst 5 for 90 min and then dilutions were plated to determine the loss of viability. *rvs161*Δ and *rvs167*Δ showed greater resistance to Hst 5 than either the wild-type or *rvs162*Δ strains at all concentrations tested. The half-maximal responses indicated a 5.9-fold resistance for *rvs161*Δ and a 10.3-fold resistance for *rvs167*Δ. Each data point represents the average of the results from three independent experiments. Bars indicate standard errors. Strains used were YLD14 (*rvs161*Δ), YLD22 (*rvs162*Δ), YLD16 (*rvs167*Δ), and wild-type DIC185.

DIC185 into the lateral tail vein become moribund in 2 to 3 days. Similar results were observed for mice infected with the *rvs162*Δ mutant. In contrast, all mice infected with either the *rvs161*Δ or *rvs167*Δ mutant strains survived beyond 10 days, with some mice remaining viable at the completion of the assay at 28 days (Fig. 7). The defects were complemented by the reintroduction of a wild-type copy of the corresponding gene.

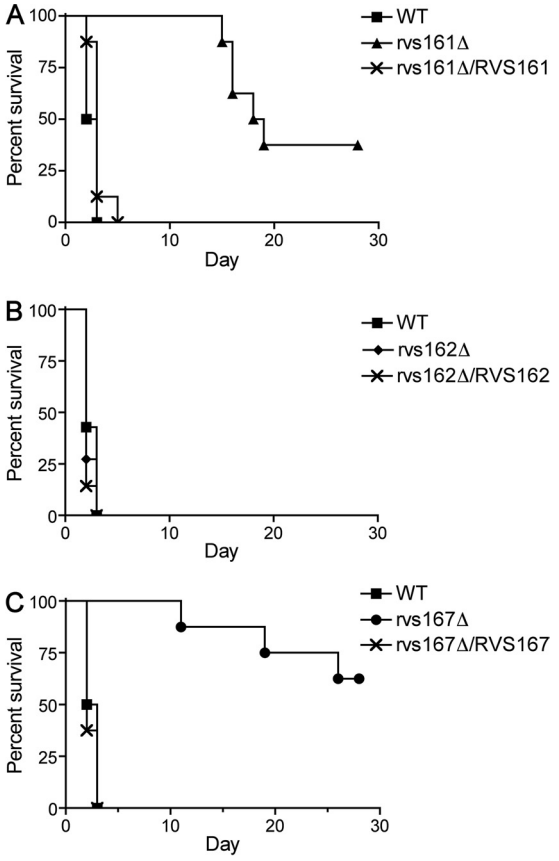

FIG. 7. Attenuated virulence of *rvs161*Δ and *rvs167*Δ mutants in a mouse model of hematogenously disseminated candidiasis. Survival curves of mice infected with *rvs161*Δ (A), *rvs162*Δ (B), or *rvs167*Δ (C) compared with that of the wild-type strain DIC185. Note the reduced virulence of the *rvs161*Δ and *rvs167*Δ strains ($P = 0.0001$). The difference between the *rvs161*Δ and *rvs167*Δ strains was not statistically different. Strains used were YLD14 (*rvs161*Δ), YLD22 (*rvs162*Δ), YLD16 (*rvs167*Δ), YLD11 (*rvs161*Δ/*rvs161*Δ/*RVS161*), YLD12 (*rvs167*Δ/*rvs167*Δ/*RVS167*), and wild-type DIC185.

The growth rate of the *rvs161*Δ mutant at 37°C in vitro was similar to that of the wild type (doubling time, 1.1 h versus 1 h), but the *rvs167*Δ mutant grew significantly slower (doubling time, 1.5 h), which could contribute to its virulence defect.

The fungal burden per gram of kidney tissue was assessed, because kidneys are the major target organs of hematogenously disseminated *C. albicans* in mice (Fig. 8A). Although the wild-type strain resulted in the highest level of CFU per gram, surprisingly, some *rvs161*Δ- and *rvs167*Δ-infected mice maintained comparatively high levels of CFU as well and still survived the entire 28-day period of the experiment. Other mice that also survived the assay to day 28 exhibited low CFU levels, apparently having cleared the majority of the fungal cells from the kidney.

To better understand the defects of the *rvs161*Δ and *rvs167*Δ mutants, the fungal load in the kidneys was analyzed after 2 and 3 days of infection. Mice infected with the wild-type strain succumbed to infection at day 2 with a median of 9.7×10^6 CFU/g kidney. Mice infected with *rvs161*Δ appeared to show a reduced fungal load (median CFU/g kidney was 1.1×10^6/g at day 2 and 0.12×10^6/g at day 3); however, these results were

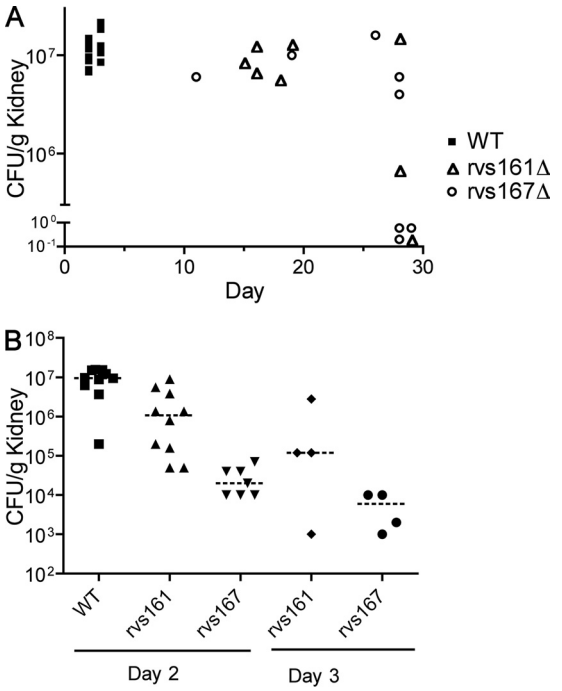

FIG. 8. Fungal load in infected kidneys. (A) Determination of CFU per gram of kidney tissue in mice that became moribund on the indicated day of infection or after euthanasia on day 28 of infection. (B) Determination of CFU per gram of kidney tissue in mice that were euthanized after 2 or 3 days of infection, as indicated. Strains used were YLD14 (*rvs161*Δ), YLD16 (*rvs167*Δ), and wild-type DIC185.

not statistically significant from those for the wild type ($P > 0.05$). In the case of the *rvs167*Δ mutant, the CFU/g kidney were 0.02×10^6/g after day 2 and 0.006×10^6/g after day 3, which were significantly different from those of the wild type ($P < 0.001$). Thus, the *rvs167*Δ mutants are defective in initiating an infection but can still grow to higher levels and cause a lethal infection. Although it appears that the CFU/g kidney in the mutants decreased between day 2 and day 3, this was not statistically significant.

A histopathological analysis of formaldehyde-fixed kidney tissue sections using PAS staining revealed that the wild type and the complemented strains caused widely disseminated infections, with large numbers of hyphal filaments emanating from discrete foci that penetrated throughout the organ (Fig. 9A). In contrast, in mice surviving to day 28, the *rvs161*Δ and *rvs167*Δ mutants grew in the center of the kidney and were not disseminated to the outer cortex. These large zones of fungal growth for the *rvs161*Δ and *rvs167*Δ mutants were surrounded by layers of leukocytes, separating the areas of infection from the remaining healthy tissue, which presumably helps to contain the dissemination of the *rvs*Δ mutants. Both the *rvs161*Δ and *rvs167*Δ mutants were capable of forming filamentous cells in vivo in spite of their apparent defects in vitro. However, some kidney sections of mice infected for 28 days with *rvs167*Δ showed mainly shorter, pseudohyphal filaments rather than the longer true hyphae. This was mainly seen in zones adjacent to partially cleared areas of the kidney (Fig. 9A), and not throughout the kidney, suggesting that it may relate to an intermediate stage in which the infection is being cleared.

The morphogenesis of the mutants was examined in more detail by staining kidney homogenates with calcofluor white, which specifically stains fungal cell wall chitin but not human tissues which lack chitin. Wild-type *C. albicans* cells were present mainly in elongated filamentous growth forms, although pseudohyphal and round blastospore-type cells were also common. Interestingly, the *rvs161*Δ and *rvs167*Δ mutants also formed extensive filamentous growth in the kidney and even appeared to form some true hyphae. However, on close examination, it was obvious that the mutants formed a higher proportion of chains of pseudohyphal cells rather than true hyphae than the wild type. Thus, altered morphogenesis may contribute to the virulence defect of the *rvs161*Δ and *rvs167*Δ mutants in vivo.

DISCUSSION

Rvs proteins are important for virulence. The *rvs161*Δ and *rvs167*Δ mutants showed greatly reduced virulence in a mouse model of candidiasis (Fig. 7). For the *rvs167*Δ mutant, this is due in part to a decreased ability to colonize the kidney (Fig. 8B). This defect is interesting, given that *rvs167*Δ typically showed a milder phenotype than *rvs161*Δ in other assays. However, an exception is that *rvs167*Δ grew more poorly than *rvs161*Δ in the presence of 5 mM H_2O_2 (Table 2), suggesting that greater sensitivity to oxidative damage by the immune system may impair its ability to initiate an infection. Over time both the *rvs161*Δ and *rvs167*Δ mutants were capable of growing to high levels in the kidney, and about half the infected mice succumbed to infection by day 28. A histological analysis of kidney sections from mice that survived to day 28 showed that the *rvs161*Δ and *rvs167*Δ infections were confined to large internal regions surrounded by layers of leukocytes (Fig. 9A), which contrasts with the highly disseminated infection by wild-type *C. albicans*. This clustering presumably accounts for why mice with comparatively high fungal burdens of *rvs161*Δ or *rvs167*Δ cells still demonstrated normal behavior. It is surprising that the *rvs161*Δ and *rvs167*Δ mutants grow well in vivo, given that endocytosis is thought to influence a wide range of properties by regulating the plasma membrane composition and the stability of nutrient sensors and other components.

Relationship between morphogenesis and virulence. The defects of the *rvs*Δ mutants in hyphal morphogenesis and invasive growth also appear to contribute to decreased virulence. Endocytosis and morphogenesis are interrelated; efficient endocytosis is thought to be critical for the appropriate localization of proteins required for polarized morphogenesis (35). Consistent with this, *rvs161*Δ was more defective than *rvs167*Δ in both endocytosis and hyphal morphogenesis, and a similar correlation was reported for mutations in other *C. albicans* genes, including *WAL1*, *SLA2*, and *MYO5* (29, 30, 43). Interestingly, the *rvs161*Δ and *rvs167*Δ mutants formed extensive filamentous growth in the kidney, suggesting that stronger inducing signals in vivo improved filamentous growth (Fig. 9). However, the mutants more frequently formed chains of elongated pseudohyphae rather than true hyphae with parallel walls. The abnormal morphogenesis of the *rvs*Δ mutants also correlates with strong defects in invasive growth into agar (Fig. 2C). The reduced ability to grow invasively may account for why the *rvs161*Δ and *rvs167*Δ mutants were primarily detected

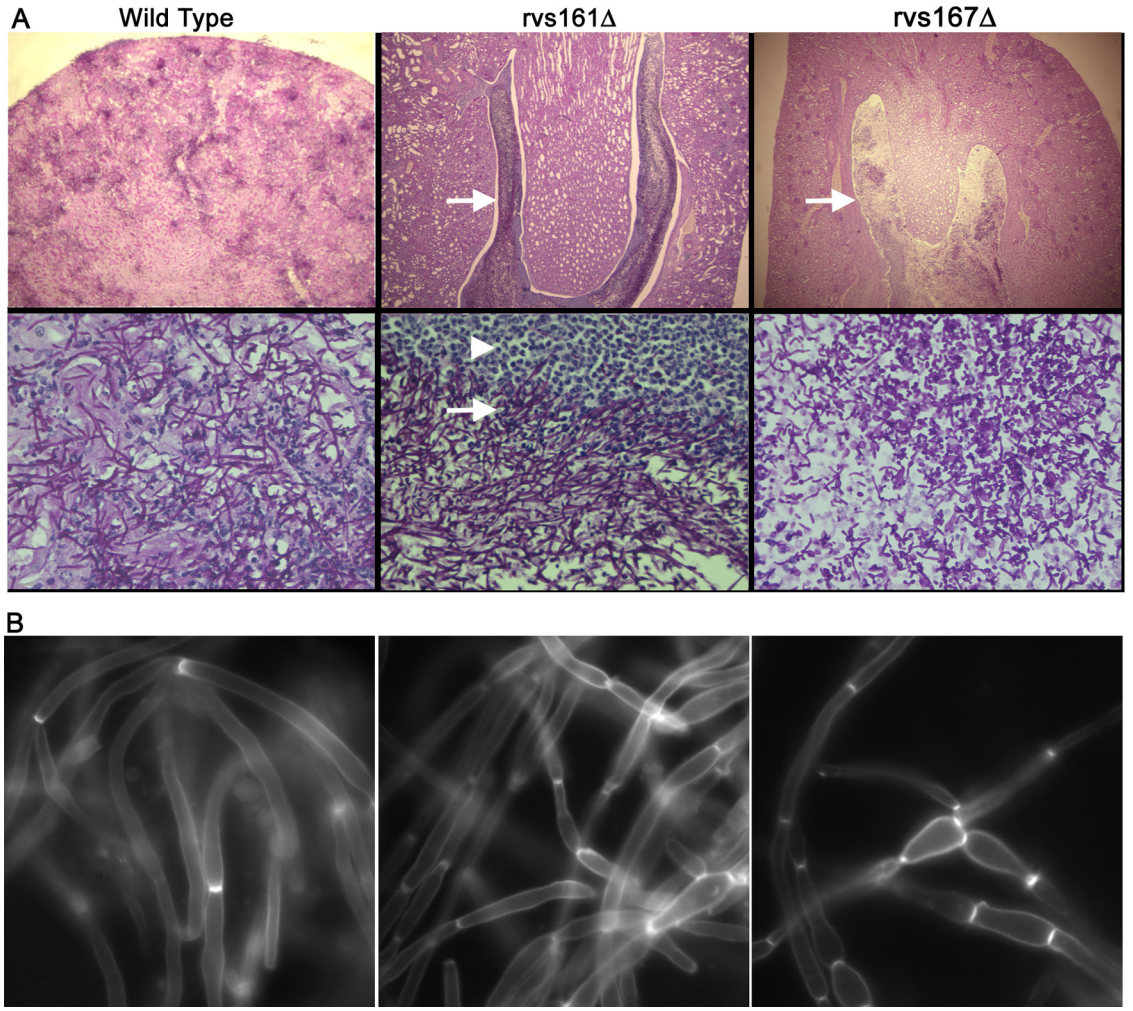

FIG. 9. Microscopic analysis of infected kidney tissue. Kidneys were excised from mice infected with the wild-type strain (DIC185) for 2 days or with the indicated *rvs*Δ mutant strain that were euthanized after 28 days of infection. (A) Kidney sections were analyzed by PAS staining. Kidney tissue infected with the DIC185 wild-type strain demonstrated a high level of penetration by hyphal filaments emanating from multiple sites within the cortex. In contrast, tissue infected with the mutant YLD14 (*rvs161*Δ) and YLD16 (*rvs167*Δ) strains showed large internal zones of fungal cells (indicated by arrows) that were completely surrounded by leukocytes (indicated by the arrowhead). Note that the zone of clearing within the fungal mass of the YLD16 (*rvs167*Δ) strain contained cells with a bud or pseudohyphal morphology. Images in the top panels were captured through a 4× lens, and the bottom panels were captured through a 60× lens. (B) Kidney homogenates were stained with calcofluor, treated with 1% KOH to help dissolve host tissues, and then examined by fluorescence microscopy.

in the central renal space and did not disseminate to the more solid cortex tissue. In agreement with this, other mutants that are defective in invasive growth in vitro, such as the *cdc10*Δ and *cdc11*Δ septin mutants, also grew as a large fungal mass in the central region of the kidney (44).

The impairment of endocytosis and morphogenesis in the *rvs*Δ mutants may also lead to the exposure of cell wall determinants recognized by the host immune system receptors. The *ScRVS161* and *ScRVS167* genes were reported to be members of a cell wall remodeling network that is essential for masking the proinflammatory inner β-glucan layer with a covering of mannan (46). The *Carvs161*Δ and *Carvs167*Δ mutants also displayed features of altered cell wall synthesis, since they were more sensitive to the cell wall-perturbing agents Congo red and calcofluor white (Table 2). Altered cell walls may help to recruit the leukocytes that were observed to surround the large mass of *rvs*Δ mutant growth in the kidney (Fig. 9). Similarly, the *Cacdc10*Δ and *Cacdc11*Δ septin mutants showed cell wall alterations and grew as large fungal masses surrounded by leukocytes in the kidney (44, 45). Thus, the cell wall defects of the *rvs*Δ and septin mutants may recruit leukocytes that help to prevent the dissemination of fungal growth.

It was suggested previously that endocytosis may also play a role in forming a special lipid domain at the hyphal tips (25, 30), which is thought to contribute to highly polarized hyphal morphogenesis and may influence the response to antifungal drugs (2). Surprisingly, the *rvs*Δ strains still exhibited enriched filipin staining of sterols at the hyphal tips (Fig. 5 and data not shown), indicating that efficient endocytosis is not required for lipid polarization. The failure of the previously described endocytosis-defective *myo5*Δ and *sla2*Δ mutants to show polarized filipin staining in response to hyphal inducers may be due

to their more severe defect in actin organization (30). Actin filaments are important for polarized filipin staining (25). In contrast to the severely defective *myo5*Δ and *sla2*Δ mutants, the *rvs*Δ mutants showed detectable actin cables (Fig. 4) and were still able to undergo more highly polarized, albeit abnormal, hyphal growth.

***RVS* genes affect susceptibility to antifungal agents and environmental conditions.** Testing with antifungal drugs that alter plasma membrane functions (32) showed that *rvs161*Δ was more sensitive to fluconazole (Fig. 7A), which blocks an intermediate step in ergosterol synthesis and results in the accumulation of toxic sterol intermediates in the membrane. The mutation of *C. albicans VPS28* and *VPS32*, vacuolar protein sorting (Vps) factors that are important in the late stages of endocytosis, also caused increased sensitivity to azoles (9). Endocytosis defects may increase sensitivity to fluconazole by altering membrane lipids or the function of multidrug transporters. However, the *rvs167*Δ mutant displayed a more complex phenotype. It was partially sensitive to low concentrations but still grew well with higher doses of fluconazole that inhibited the wild-type strain (Fig. 7). Thus, the different effects of the *rvs*Δ mutations on fluconazole sensitivity are likely due in part to other functions and not simply to endocytosis.

An analysis of the growth of the *Carvs*Δ mutants under different environmental conditions revealed additional phenotypes that likely influence the virulence of these strains (Table 2). Both *rvs161*Δ and *rvs167*Δ cells were more resistant to Hst 5, an antimicrobial peptide that acts in the oropharyngeal environment, which is consistent with a proposed role for endocytosis in its uptake (17, 23, 51). Both *rvs161*Δ and *rvs167*Δ were more sensitive to H_2O_2, which likely makes them more sensitive to attack by the immune system. The *rvs161*Δ and *rvs167*Δ mutants were also more sensitive to an alkaline pH (pH 8.5) and to 0.15 M LiCl, which are hallmarks of mutants in the RIM101 pH response pathway (11). Interestingly, ESCRT-III complex mutants that are defective in the later stages of endocytosis are also defective in the RIM101 pH response pathway (20, 50).

Surprisingly, although the *Carvs*Δ and *Scrvs*Δ mutants shared many similarities, they displayed some opposite phenotypes in that the *Carvs161*Δ and *Carvs167*Δ mutants were sensitive to calcofluor white and Congo red (6) but not to elevated NaCl (4). Thus, although the *rvs*Δ mutations result in altered cell wall function in both organisms, they do so in different ways. Furthermore, the *Carvs*Δ strains did not show the "reduced viability upon nutrient starvation" phenotype (Table 2) for which the *Scrvs* mutants were originally named (10).

Altogether, the analysis of the *RVS* genes in *C. albicans* indicates that endocytic mechanisms play diverse roles in promoting efficient virulence in mice. This is consistent with the fundamental role of endocytosis in regulating the plasma membrane, which is an important site for interfacing with the host environment and for regulating growth and morphogenesis. Although the *rvs161*Δ and *rvs167*Δ mutants could still grow well in vivo, their strong defects in virulence indicate that endocytosis could be targeted to diminish dissemination and to sensitize cells to antifungal therapy.

ACKNOWLEDGMENTS

We thank Aaron Mitchell, Judith Berman, Amy Warenda, and Scott Filler for the plasmids and strains and James Bliska for advice. We also thank Kenneth Shroyer for advice on interpreting the histopathology studies.

This work was supported by grant RO1 AI47837 from the National Institutes of Health that was awarded to J.B.K.

REFERENCES

1. **Adams, A. E. M., and J. R. Pringle.** 1991. Staining of actin with fluorochrome-conjugated phalloidin. Methods Enzymol. **194:**729–731.
2. **Alvarez, F. J., L. M. Douglas, and J. B. Konopka.** 2007. Sterol-rich plasma membrane domains in fungi. Eukaryot. Cell **6:**755–763.
3. **Alvarez, F. J., L. M. Douglas, A. Rosebrock, and J. B. Konopka.** 2008. The Sur7 protein regulates plasma membrane organization and prevents intracellular cell wall growth in *Candida albicans*. Mol. Biol. Cell **19:**5214–5225.
4. **Balguerie, A., M. Bagnat, M. Bonneu, M. Aigle, and A. M. Breton.** 2002. Rvs161p and sphingolipids are required for actin repolarization following salt stress. Eukaryot. Cell **1:**1021–1031.
5. **Blankenship, J. R., and A. P. Mitchell.** 2006. How to build a biofilm: a fungal perspective. Curr. Opin. Microbiol. **9:**588–594.
6. **Breton, A. M., J. Schaeffer, and M. Aigle.** 2001. The yeast Rvs161 and Rvs167 proteins are involved in secretory vesicles targeting the plasma membrane and in cell integrity. Yeast **18:**1053–1068.
7. **Calderone, R. A., and W. A. Fonzi.** 2001. Virulence factors of *Candida albicans*. Trends Microbiol. **9:**327–335.
8. **Casamayor, A., and M. Snyder.** 2003. Molecular dissection of a yeast septin: distinct domains are required for septin interaction, localization, and function. Mol. Cell. Biol. **23:**2762–2777.
9. **Cornet, M., C. Gaillardin, and M. L. Richard.** 2006. Deletions of the endocytic components *VPS28* and *VPS32* in *Candida albicans* lead to echinocandin and azole hypersensitivity. Antimicrob. Agents Chemother. **50:**3492–3495.
10. **Crouzet, M., M. Urdaci, L. Dulau, and M. Aigle.** 1991. Yeast mutant affected for viability upon nutrient starvation: characterization and cloning of the *RVS161* gene. Yeast **7:**727–743.
11. **Davis, D.** 2003. Adaptation to environmental pH in *Candida albicans* and its relation to pathogenesis. Curr. Genet. **44:**1–7.
12. **Dawson, J. C., J. A. Legg, and L. M. Machesky.** 2006. Bar domain proteins: a role in tubulation, scission and actin assembly in clathrin-mediated endocytosis. Trends Cell Biol. **16:**493–498.
13. **Engqvist-Goldstein, A. E., and D. G. Drubin.** 2003. Actin assembly and endocytosis: from yeast to mammals. Annu. Rev. Cell Dev. Biol. **19:**287–332.
14. **Friesen, H., K. Colwill, K. Robertson, O. Schub, and B. Andrews.** 2005. Interaction of the Saccharomyces cerevisiae cortical actin patch protein Rvs167p with proteins involved in ER to Golgi vesicle trafficking. Genetics **170:**555–568.
15. **Friesen, H., K. Murphy, A. Breitkreutz, M. Tyers, and B. Andrews.** 2003. Regulation of the yeast amphiphysin homologue Rvs167p by phosphorylation. Mol. Biol. Cell **14:**3027–3040.
16. **Germann, M., E. Swain, L. Bergman, and J. T. Nickels, Jr.** 2005. Characterizing the sphingolipid signaling pathway that remediates defects associated with loss of the yeast amphiphysin-like orthologs, Rvs161p and Rvs167p. J. Biol. Chem. **280:**4270–4278.
17. **Helmerhorst, E. J., P. Breeuwer, W. van't Hof, E. Walgreen-Weterings, L. C. Oomen, E. C. Veerman, A. V. Amerongen, and T. Abee.** 1999. The cellular target of histatin 5 on *Candida albicans* is the energized mitochondrion. J. Biol. Chem. **274:**7286–7291.
18. **Hicke, L.** 1999. Gettin' down with ubiquitin: turning off cell-surface receptors, transporters and channels. Trends Cell Biol. **9:**107–112.
19. **Kaksonen, M., C. P. Toret, and D. G. Drubin.** 2005. A modular design for the clathrin- and actin-mediated endocytosis machinery. Cell **123:**305–320.
20. **Kullas, A. L., M. Li, and D. A. Davis.** 2004. Snf7p, a component of the ESCRT-III protein complex, is an upstream member of the RIM101 pathway in *Candida albicans*. Eukaryot. Cell **3:**1609–1618.
21. **Kumamoto, C. A., and M. D. Vinces.** 2005. Contributions of hyphae and hypha-co-regulated genes to *Candida albicans* virulence. Cell. Microbiol. **7:**1546–1554.
22. **Li, X. S., M. S. Reddy, D. Baev, and M. Edgerton.** 2003. *Candida albicans* Ssa1/2p is the cell envelope binding protein for human salivary histatin 5. J. Biol. Chem. **278:**28553–28561.
23. **Li, X. S., J. N. Sun, K. Okamoto-Shibayama, and M. Edgerton.** 2006. *Candida albicans* cell wall ssa proteins bind and facilitate import of salivary histatin 5 required for toxicity. J. Biol. Chem. **281:**22453–22463.
24. **Lombardi, R., and H. Riezman.** 2001. Rvs161p and Rvs167p, the two yeast amphiphysin homologs, function together in vivo. J. Biol. Chem. **276:**6016–6022.
25. **Martin, S. W., and J. B. Konopka.** 2004. Lipid raft polarization contributes to hyphal growth in *Candida albicans*. Eukaryot. Cell **3:**675–684.

26. **Martin, S. W., and J. B. Konopka.** 2004. SUMO modification of septin-interacting proteins in *Candida albicans*. J. Biol. Chem. **279:**40861–40867.
27. **Mochon, A. B., and H. Liu.** 2008. The antimicrobial peptide histatin-5 causes a spatially restricted disruption on the *Candida albicans* surface, allowing rapid entry of the peptide into the cytoplasm. PLoS Pathog. **4:**e1000190.
28. **Munn, A. L., B. J. Stevenson, M. I. Geli, and H. Riezman.** 1995. *end5*, *end6*, and *end7*: mutations that cause actin delocalization and block the internalization step of endocytosis in *Saccharomyces cerevisiae*. Mol. Biol. Cell **6:**1721–1742.
29. **Oberholzer, U., T. L. Iouk, D. Y. Thomas, and M. Whiteway.** 2004. Functional characterization of myosin I tail regions in *Candida albicans*. Eukaryot. Cell **3:**1272–1286.
30. **Oberholzer, U., A. Nantel, J. Berman, and M. Whiteway.** 2006. Transcript profiles of *Candida albicans* cortical actin patch mutants reflect their cellular defects: contribution of the Hog1p and Mkc1p signaling pathways. Eukaryot. Cell **5:**1252–1265.
31. **Odds, F. C.** 1988. *Candida* and candidosis. Bailliere Tindall, Philadelphia, PA.
32. **Odds, F. C., A. J. Brown, and N. A. Gow.** 2003. Antifungal agents: mechanisms of action. Trends Microbiol. **11:**272–279.
33. **Park, H., C. L. Myers, D. C. Sheppard, Q. T. Phan, A. A. Sanchez, J. E. Edwards, Jr., and S. G. Filler.** 2005. Role of the fungal Ras-protein kinase A pathway in governing epithelial cell interactions during oropharyngeal candidiasis. Cell. Microbiol. **7:**499–510.
34. **Pringle, J. R.** 1991. Staining of bud scars and other cell wall chitin with calcofluor. Methods Enzymol. **194:**732–735.
35. **Pruyne, D., and A. Bretscher.** 2000. Polarization of cell growth in yeast. J. Cell Sci. **113:**571–585.
36. **Raj, P. A., M. Edgerton, and M. J. Levine.** 1990. Salivary histatin 5: dependence of sequence, chain length, and helical conformation for candidacidal activity. J. Biol. Chem. **265:**3898–3905.
37. **Sewell, D. L., M. A. Pfaller, and A. L. Barry.** 1994. Comparison of broth macrodilution, broth microdilution, and E test antifungal susceptibility tests for fluconazole. J. Clin. Microbiol. **32:**2099–2102.
38. **Sherman, F.** 2002. Getting started with yeast. Methods Enzymol. **350:**3–41.
39. **Sudbery, P., N. Gow, and J. Berman.** 2004. The distinct morphogenic states of *Candida albicans*. Trends Microbiol. **12:**317–324.
40. **Valdez-Taubas, J., and H. R. Pelham.** 2003. Slow diffusion of proteins in the yeast plasma membrane allows polarity to be maintained by endocytic cycling. Curr. Biol. **13:**1636–1640.
41. **Veerman, E. C., M. Valentijn-Benz, K. Nazmi, A. L. Ruissen, E. Walgreen-Weterings, J. van Marle, A. B. Doust, W. van't Hof, J. G. Bolscher, and A. V. Amerongen.** 2007. Energy depletion protects *Candida albicans* against antimicrobial peptides by rigidifying its cell membrane. J. Biol. Chem. **282:**18831–18841.
42. **Vida, T. A., and S. D. Emr.** 1995. A new vital stain for visualizing vacuolar membrane dynamics and endocytosis in yeast. J. Cell Biol. **128:**779–792.
43. **Walther, A., and J. Wendland.** 2004. Polarized hyphal growth in *Candida albicans* requires the Wiskott-Aldrich syndrome protein homolog Wal1p. Eukaryot. Cell **3:**471–482.
44. **Warenda, A. J., S. Kauffman, T. P. Sherrill, J. M. Becker, and J. B. Konopka.** 2003. *Candida albicans* septin mutants are defective for invasive growth and virulence. Infect. Immun. **71:**4045–4051.
45. **Warenda, A. J., and J. B. Konopka.** 2002. Septin function in *Candida albicans* morphogenesis. Mol. Biol. Cell **13:**2732–2746.
46. **Wheeler, R. T., and G. R. Fink.** 2006. A drug-sensitive genetic network masks fungi from the immune system. PLoS Pathog. **2:**e35.
47. **Whiteway, M., and U. Oberholzer.** 2004. *Candida* morphogenesis and host-pathogen interactions. Curr. Opin. Microbiol. **7:**350–357.
48. **Wilson, R. B., D. Davis, B. M. Enloe, and A. P. Mitchell.** 2000. A recyclable *Candida albicans URA3* cassette for PCR product-directed gene disruptions. Yeast **16:**65–70.
49. **Wilson, R. B., D. Davis, and A. P. Mitchell.** 1999. Rapid hypothesis testing with *Candida albicans* through gene disruption with short homology regions. J. Bacteriol. **181:**1868–1874.
50. **Xu, W., F. J. Smith, Jr., R. Subaran, and A. P. Mitchell.** 2004. Multivesicular body-ESCRT components function in pH response regulation in *Saccharomyces cerevisiae* and *Candida albicans*. Mol. Biol. Cell **15:**5528–5537.
51. **Zhu, J., P. W. Luther, Q. Leng, and A. J. Mixson.** 2006. Synthetic histidine-rich peptides inhibit *Candida* species and other fungi in vitro: role of endocytosis and treatment implications. Antimicrob. Agents Chemother. **50:**2797–2805.
52. **Zimmerberg, J., and S. McLaughlin.** 2004. Membrane curvature: how BAR domains bend bilayers. Curr. Biol. **14:**R250–R252.

Editor: A. Casadevall